The current issue and full text archive of this journal is available at
www.emeraldinsight.com/0961-5539.htm

Received 14 May 2007
Revised 28 February 2008
Accepted 28 February 2008

Finite element numerical analysis of blood flow and temperature distribution in three-dimensional image-based finger model

Ying He
Department of Modern Mechanics, University of Science and Technology of China, Hefei, China and Computational Biomechanics Unit, RIKEN, Saitama, Japan
Ryutaro Himeno
Computational Biomechanics Unit, RIKEN, Saitama, Japan
Hao Liu
Computational Biomechanics Unit, RIKEN, Saitama, Japan and Faculty of Engineering, Chiba University, Chiba, Japan
Hideo Yokota
Computational Biomechanics Unit, RIKEN, Saitama, Japan, and
Zhi Gang Sun
Advanced Simulation Technology of Mechanics Co. Ltd, Saitama, Japan

Abstract

Purpose – The purpose of this paper is to investigate the blood flow and temperature distribution in human extremities.

Design/methodology/approach – The simulation is carried out from three aspects. Firstly, the hemodynamics in the human upper limb is analyzed by one-dimensional model for pulsalite flow in an elastic tube. Secondly, the blood flow and heat transfer through living tissues are described basing on porous media theory, and the tissue model is coupled with the one-dimensional blood flow model. With respect to geometric modeling, MR-image-based modeling method is employed to construct a realistic model of the human finger.

Findings – It is found that the temperature variation is closely related to the blood flow variation in the fingertip and the blood flow distribution in the tissue is dependent on the locations of large arteries and veins.

Originality/value – Blood flow and temperature distribution in a 3D realistic human finger are firstly obtained by coupling the blood circulation and porous media model.

Keywords Flow, Porous materials, Finite element analysis, Blood, Limbs, Temperature

Paper type Research paper

International Journal of Numerical Methods for Heat & Fluid Flow
Vol. 18 No. 7/8, 2008
pp. 932-953

0961-5539
DOI 10.1108/09615530810899033

The first author would like to thank Ms J. Sunaga and Mr N. Kakusho for the support with taking MR images. The work was supported in part by KAKENHI of JSPS, Research (C), No. 18560218.

1. Introduction

The human finger has a high-sensory capability that can convey information about mechanical, thermal, and tissue-damaging events. It has been known that the finger skin temperature is closely related to the total digital blood flow; for example, after cigarette smoking, peripheral circulation degrades and skin temperature decreases (Bornmyr and Svensson, 1991). When people are in a state of stress, the finger skin temperature decreases for the vasoconstriction of finger arterioles (Nketia and Reisman, 1997). While warming distant torso body areas, blood circulation to the fingers is augmented and temperature of fingers increases to a comfortable level during exposure to cold (Koscheyev *et al.*, 2000). Owing to the human finger's high-sensory capability, it has potential applications in developing new health care instruments. For instance, Cho *et al.* (2004) proposed a noninvasive method for measuring glucose, where glucose was derived by measuring heat generation, blood flow rate, and hemoglobin oxygenation in a person's fingertip.

Owing to the unique characteristics in hemodynamics and thermoregulation and potential applications, developing a computational model of the human extremity or human body that can simulate the physiological characteristics is always a subject for further investigation.

Yokoyama and Ogino (1985) put forward a computer model to investigate cold-stressed effects on the finger. They developed a physiological model of the finger according to measurements and anatomical structure. The finger was modeled in the shape of a cylinder comprising several layers, including bone, tendon, and skin. The heat transfer process was depicted by three equations: those for heat transport processes in tissue, arterial, and venous pools.

Ling *et al.* (1995) proposed a finite element (FE) model to investigate the cooling effects of water bags on a human leg. The modeled leg comprised skin, fat, bones, and two main arteries. The Pennes bio-heat equation was used, and the blood perfusion term was assumed to be a function of the local tissue temperature. They considered the blood flow inside main arteries as non-Newtonian laminar flow.

Shitzer *et al.* (1997) presented a thermal model of an extremity such as a finger. This model includes not only the effects of heat conduction, metabolic heat generation, and heat transport by blood perfusion, but also heat exchange between tissue and larger blood vessels and arterio-venous heat exchange. The heat transfer coefficient for major blood vessels is derived from the relationship between the blood vessel radius, "influence volume" radius, cylinder radius, and thermal conductivity.

Researchers also tried to investigate global thermoregulation behavior by constructing a global thermoregulation model. Takemori *et al.* (1995) proposed a thermal model for predicting human comfort in an indoor environment. In their model, the human body was modeled into several cylinders and every cylinder was connected by a circulatory system. The respiratory system was also considered in their model. Salloum *et al.* (2005) provided a similar thermal model that included 15 cylindrical parts and whose circulatory system was considered in greater detail. In each body segment, the blood exiting from the arteries was divided into blood flowing into the core and blood flowing into the skin layer. The opposite action occurred in the veins of the same segment. The model was used to predict the nude body temperature during different ambient conditions and activities.

The common characteristics of the above models are that they used one or several cylinders to model the geometry of the human body and their governing equations were developed from the Pennes (1948) equation, but the hemodynamics of the circulation system was still not considered.

On the other hand, a blood-perfused biological tissue can be described as a porous media in which the fluid phase represents the blood and the surrounding tissue is represented by the solid phase. The theory of porous media for heat transfer in living tissues may be the most appropriate since it can describe the perfused blood with fewer assumptions as compared to other bioheat models (Khaled and Vafai, 2003). Wulff (1974) first dealt with the living tissue as a porous medium and utilized the convective term, including the Darcy velocity, to replace the blood perfusion term in the bioheat equation. Xuan and Roetzel (1997) used the transport theory through porous media to model a tissue-blood system and analyzed the temperature distribution in human upper limbs. Blood and tissue were considered to be in a nonequilibrium state, and two energy equations were used to express heat transfer in the blood phase and solid phase. The advantage of this model is that it includes the exact blood perfusion in tissues, blood dispersion, and effective tissue conductivity, and it is considered to be appropriate for modeling a blood-perfused tissue with fewer assumptions. However, the flow in large blood vessels differs from that through tissues and may be considered separately.

Besides, modeling heat ransfer in living tissue, modeling the detailed countercurrent microvascular network is also of significance. Chen and Homles (1980) treated the blood vessels as two groups in their model – large and small vessels. Each vessel is treated separately in the former group, whereas all vessels are treated as a part of a continuum in the latter group. The thermal contributions of the small blood vessels were considered from the equilibration of blood temperature, convection of the flowing blood, and the small temperature fluctuations of the nearly equilibrated blood. Weibaum and Jiji (1985) proposed an alternative model that accounts for the thermal effect of the directionality of the blood vessels and the characteristic geometry of the blood vessel arrangement. The vascular structure in the periphery was treated individually rather than as continuum media in their three-layer model.

One-dimensional nonlinear fluid model has been widely used to simulate the human blood circulation system (arteries, capillaries, and veins). For example, a global mathematical model of cerebral circulation in humans presented by Zagzoule and Marc-Vergnes (1986) a computational model to investigate the behavior of the entire human systemic circulation developed by Sheng *et al.* (1995) and structured-tree systemic arterial model presented by Olufsen *et al.* (2000). Applying the hemodynamic model to the thermal analysis of blood blow may be an alternative method. He *et al.* (2004) focused their attention on the heat transfer of blood flow by developing a one-dimensional thermifluid model.

With the development of image processing and mesh generation technique, using realistic geometric computational models to analyze the biomechanical characteristics is becoming a tendency. Fukuda *et al.* (2005) investigated the deformation of the soft tissue in the fingertip using a 3D realistic computational model constructed from CT images. Reynolds *et al.* (2006) have constructed an accurate geometric model of the forearm and hand muscles and they intend to apply the model to analyze the

mechanical motions of the forearm and the hand, along with the associated muscle movement. He *et al.* (2006) concentrated their efforts in this area by using a realistic 2D finger model constructed from MR images to investigate the blood flow and temperature distribution based on the transport theory in porous media.

The purpose of this study is to model blood-tissue heat transfer according to the different characteristics of blood flow in large vessels and tissues from three aspects. First, systemic blood circulation in the upper limb has been modeled based on one-dimensional flow in an elastic tube. Second, the 3D FE model based on heat transport in porous media has been developed to analyze the blood perfusion and heat transport in the human finger. Further, a realistic 3D geometric model for the human finger has been constructed on the basis of MR image data. By coupling the one-dimensional blood flow model and the porous media model, the blood pressure, velocity, and temperature of blood and tissues in a human finger were simulated.

2. Modeling blood flow dynamics and heat transfer in tissues

The basic concept in modeling blood flow is the use of different models to simulate blood flow in large vessels (with diameters greater than or equal to 1 mm) and in microvessels. A nonlinear one-dimensional thermo-fluid model in an elastic tube is used to express blood flow in large vessels, and blood flow perfused in tissues is considered as the fluid phase in porous media. The energy equation for porous media is used to model the heat transfer in tissues.

2.1 Blood flow dynamics

The blood flow in large vessels has been modeled as one-dimensional flow in an elastic tube, and the governing equations, including continuity and momentum, are expressed as:

$$\frac{\partial A}{\partial t} + \frac{\partial q}{\partial x} = 0, \tag{1}$$

$$\frac{\partial q}{\partial t} + \frac{\partial}{\partial x}\left(\frac{q^2}{A}\right) + \frac{A}{\rho}\frac{\partial P}{\partial x} = -\frac{2\pi\nu r}{\delta}\frac{q}{A}, \tag{2}$$

where x is the distance from the heart; t, the time; A, the cross-sectional area of the blood vessel; q, the blood flow rate; P, the transmural pressure; ρ, the blood density; ν, the kinematic viscosity; δ, the boundary-layer thickness; and r, the radius of the blood vessel.

The pressure-area relationship for the arteries and veins is as follows:

$$P(x,t) - P_0 = \frac{4}{3}\frac{Eh}{r_0}\left(1 - \sqrt{\frac{A_0}{A}}\right), \tag{3}$$

$$p - p_0 = k_p\left[1 - \left(\frac{A}{A_0}\right)^{-3/2}\right], \tag{4}$$

where E is Young's modulus; h, the wall thickness of the blood vessel; and k_p, the coefficient proportional to the bending stiffness of the tube wall.

The energy equation for the one-dimensional model is written as:

$$\frac{\partial T_b}{\partial t} + \frac{q}{A}\frac{\partial T_b}{\partial x} = -\omega T_b - \frac{h_{ves}A_s}{\rho_b c_b A}(T_b - T_{tmn}). \tag{5}$$

A periodic flow wave was assigned at the inlet boundary, and a constant pressure was assigned at the outlet. With regard to the bifurcation conditions and the junction conditions between two equivalent tubes, it was assumed that there is no leakage of blood at the bifurcations, the inflow and outflow are balanced, and the pressure is continuous.

The two-step Lax-wendroff finite difference scheme has been broadly used to compute the blood flow and cross-sectional area for the interior points of each segment of vessels in one-dimensional hemodynamic models (Zagzoule and Marc-Vergnes, 1986; Sheng *et al.*, 1995; Olufsen *et al.*, 2000; Li and Cheng, 1993). Combining boundary conditions for the pressure and flow rate at the bifurcation with this scheme, the parameters at the bifurcation points can be computed (Zagzoule and Marc-Vergnes, 1986). The same scheme as the work of Zagzoule and Marc-Vergnes (1986) was used to solve the set of nonlinear equations (He *et al.*, 2004). The computed pressure, velocity and temperature of the corresponded vessels in the finger were transferred to the FE tissue model and assigned to the nodes represented as the blood. Thus, effect of large vessels can be added in the FE tissue model.

2.2 Darcy model and energy equation for biological tissues

The Darcy model is considered to be the earliest flow transport model in porous media and is expressed as:

$$\nabla P = -\frac{\mu}{K}\boldsymbol{\nu}, \tag{6}$$

where K is the permeability of the tissues; μ, the viscosity; and $\boldsymbol{\nu}$, the Darcy velocity. Based on the assumption that there is a local thermal equilibrium between solid tissue and blood flow, the energy equation is expressed as:

$$[(1-\varphi)(\rho c_p)_s + \varphi(\rho c_p)_f]\frac{\partial T_m}{\partial t} + (\rho c_p)_f \boldsymbol{\nu}\cdot\nabla T_m$$
$$= \nabla\cdot([(1-\varphi)k_s + \varphi k_f]\nabla T_m) + [(1-\varphi)q_s + \varphi q_f], \tag{7}$$

where:

$$(\rho c)_m = \varphi(\rho c)_b + (1-\varphi)(\rho c)_t \tag{8}$$

$$k_m = \varphi k_b + (1-\varphi)k_t, \tag{9}$$

$$q_m = \varphi q_b + (1-\varphi)q_t, \tag{10}$$

are the overall heat capacity per unit volume, overall thermal conductivity, and overall heat production per unit volume of the tissue, respectively, and ϕ is the porosity of the tissue.

Considering the continuity equation and momentum equation, the dimensionless pressure in porous media is written as:

$$\frac{\partial^2 P^*}{\partial x^{*2}} + \frac{\partial^2 P^*}{\partial y^{*2}} + \frac{\partial^2 P^*}{\partial z^{*2}} = 0. \tag{11}$$

The dimensionless velocity is expressed as:

$$u^* = -Da\,\mathrm{Re}\,\frac{\partial P^*}{\partial x^*} \quad v^* = -Da\,\mathrm{Re}\,\frac{\partial P^*}{\partial y^*} \quad w^* = -Da\,\mathrm{Re}\,\frac{\partial P^*}{\partial z^*}, \tag{12}$$

where Da is the Darcy number and is expressed as:

$$Da = \frac{K}{D^2}. \tag{13}$$

The dimensionless energy equation is as follows:

$$\frac{\partial T^*}{\partial t^*} + \varepsilon\left[u^*\frac{\partial T^*}{\partial x^*} + v^*\frac{\partial T^*}{\partial y^*} + w^*\frac{\partial T^*}{\partial z^*}\right] = \frac{1}{Pe_m}\left[\frac{\partial^2 T^*}{\partial x^{*2}} + \frac{\partial^2 T^*}{\partial y^{*2}} + \frac{\partial^2 T^*}{\partial z^{*2}}\right] + \frac{1}{Pe_m} q_m^*, \tag{14}$$

where Pe_m, ε, and q_m^* are expressed as follows:

$$Pe_m = \frac{U_\infty D}{\alpha_m}, \tag{15}$$

$$\varepsilon = \frac{(\rho c)_b}{(\rho c)_m}, \tag{16}$$

$$q_m^* = \frac{q_m D^2}{(T_a - T_\infty)k_m}. \tag{17}$$

In the air, the heat rate conducted to the skin surface is equal to the heat rate to the air from the surface by convection, radiation and evaporation. Therefore, the boundary condition can be expressed as:

$$-\lambda_s \frac{\partial T}{\partial n}\bigg|_\Gamma = h_c(T^* - T_\infty^*)\big|_\Gamma + h_{ra}(T^* - T_\infty^*)\big|_\Gamma + E_{sk}^*. \tag{18}$$

The dimensionless equation is written as:

$$-\left.\frac{\partial T}{\partial n}\right|_{\Gamma} = BiT|_{\Gamma} + \frac{h_{ra}D}{\lambda_s}\, T|_{\Gamma} + E_{sk}, \tag{19}$$

where the parameter E_{sk} is expressed by:

$$E_{sk} = \frac{E^*_{sk}D}{\lambda(T^*_a - T^*_\infty)}. \tag{20}$$

When the finger is in the moving air whose velocity is in the range of $0 < V < 0.15$ m/s, the heat transfer coefficient at the surface of the finger is 4.0 W/m^{2}K. With respect to the radiative heat transfer coefficient, we used the constant value of 4.7 W/m^{2}K as representative for the typical indoor temperature (ASHRAE, 1997).

Evaporative heat loss E^*_{sk} from skin depends on the difference between water vapor pressure for the skin and for the air (Clark and Edholm, 1985). It can be written as:

$$E^*_{sk} = h_e\left(P^*_s - P^*_{amb}\right). \tag{21}$$

The evaporative coefficient can be expressed as a function of air movement (Clark and Edholm, 1985) by:

$$h_e = 124\sqrt{V^*_{amb}} \quad \text{W/m}^2\text{kPa}. \tag{22}$$

Equations (11)-(12) and (14) have been discretized using the Galerkin weighted residual method, and the conjugate gradient method was employed to solve the equations. First, the capillary pressure in tissues was computed and the value of the blood pressure in the large vessels was obtained from the one-dimensional model and was assigned as the boundary condition of equation (11). Second, the blood flow velocities in the tissues were computed and the slip condition was employed at a large vessel wall. Finally, the temperatures in large vessels and tissues were computed. A constant blood temperature condition was assigned to the inlet of the large arteries in the finger. The flowchart of the computational method is shown in Figure 1.

3. Geometrical modelling for human finger from MR images

Since we used a one-dimensional flow model to describe blood flow in arteries and veins, data of the cross-sectional area and the length of the blood vessel are required and are defined on the basis of previous works (Sheng *et al.*, 1995; Olufsen *et al.*, 2000).

3.1 MR image acquisition

The original images were acquired for a volunteer's finger. A hand-fitted supporter made of silicon rubber was produced in order to fix the volunteer's hand before taking images. A 1.5-T scanner (Excelart, Toshiba Medical Systems) was used with different sequences for taking images of blood flow and different tissues. The image resolution was 256 × 256, and the slice thickness was set to 1.0 mm. A circular coil whose diameter fit the length of the volunteer's finger was employed. Figure 2 shows the original MR cross-sectional images in different positions.

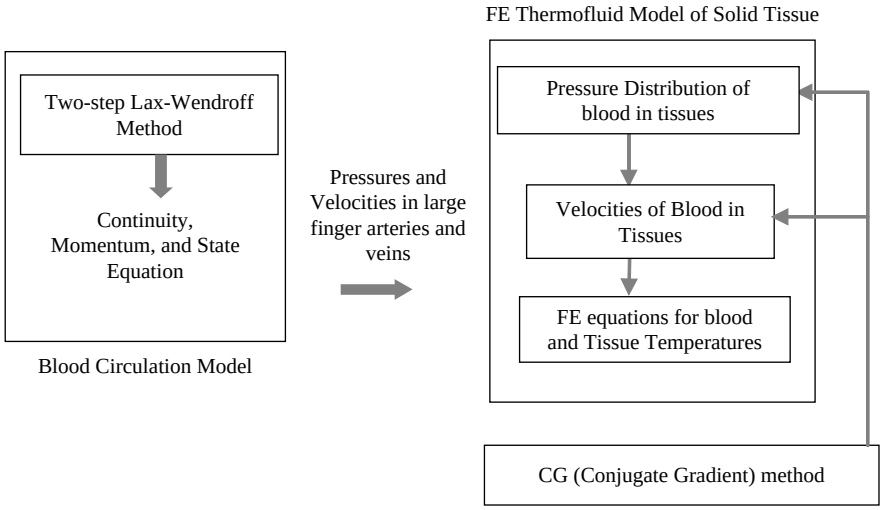

Figure 1.
Flowchart of computational method

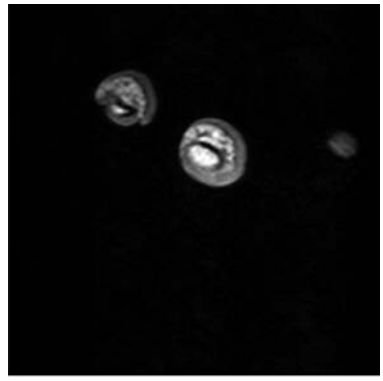

(a) Slice-No. 39

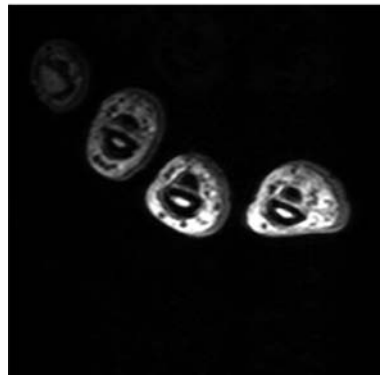

(b) Slice-No. 95

Figure 2.
Original MR cross-sectional images of human finger in different positions

3.2 Edge detection

Several image processing operators were applied in turn to reduce the noise present in the original image and to subtract the image data from the background. The image processing was carried out by an image processing and analysis program – Scion Image (www.scioncorp.com/), which supports many standard image processing functions. As regards the edge detection of the middle finger, the images of other fingers were firstly cut-off. Furthermore, smoothing, contrast enhancement, and arithmetic subtraction for the images of the middle finger were performed and the images only with the information of the objected finger were thus acquired. Figure 3 shows the processed images of the middle finger. These images were further processed manually and only the bone and skin area were segmented, whose boundaries were indicated by discrete pixels with different brightness. Figure 4 shows the final processed images corresponding to Figure 3. The processed images can be exported as text files with information about the brightness of each pixel in the images. Table I shows a part of the text file of the processed image in which the numbers represent the brightness of every pixel. The area where the brightness number was not 254 represents the finger area. The edge of the finger and the bone were set in several special values of brightness; hence, the position of the skin and the bone of the human finger can be identified by detecting these determined pixels.

(a) Slice-No. 39 **(b)** Slice-No. 95

Figure 3.
MR cross-sectional images of human finger in different positions after image processing

Figure 4.
The images after the image segmentation

254	254	254	80
254	254	254	210
254	254	210	210
254	20	210	210
254	210	210	210
254	210	210	210
254	210	210	210
20	210	210	210
210	210	210	210
210	210	210	210
20	210	210	210

Table I.
Text file of processed MR image

3.3 Mesh generation

Figure 5 shows the flow chart for the mesh generation. The text files with the image information were subsequently input into the mesh generation program. Since the text files include the color information to express different materials, for instance, the color indices 20, 70, 120, 80 express four segments of the skin boundary and the color indices 100, 30, 40, 10, 90 reveal the four segments of the bone boundary, we can identify these boundaries according to the edge information. Through this boundary information, the finger domain was subdivided into three subregions, namely, bone, tendon, and skin and muscle subdomains. Since the characteristic color indices were used to define different segments of every subdomain, the corresponding characteristic pixels on a pair of opposite sides may be connected by straight lines, and the interior grid points were generated by linear interpolation.

Grids were firstly generated on the subdomain of bone and the nodes in the interconnection with tendon were recorded in advance. Secondly, the same procedure was conducted on the tendon subdomain by using the nodes in the interconnection as the starting points. The nodes related to the boundaries of the two subregions were recorded as the inner side of the muscle region. Furthermore, the nodes in the inner side and the opposite skin side were connected by straight lines and unidirectional interpolation technique was employed for the grid generation in the third subregion. Figure 6(a)-(c) shows the 2D mesh from different processed cross-sectional images. After elements in each slice were generated, they were stacked to construct a 3D mesh. In this process, 24 slices were employed and the distance between two adjacent slices was 4 mm.

Figure 7 is result of the 3D mesh generation of the human finger. The main program for mesh generation is listed in Appendix.

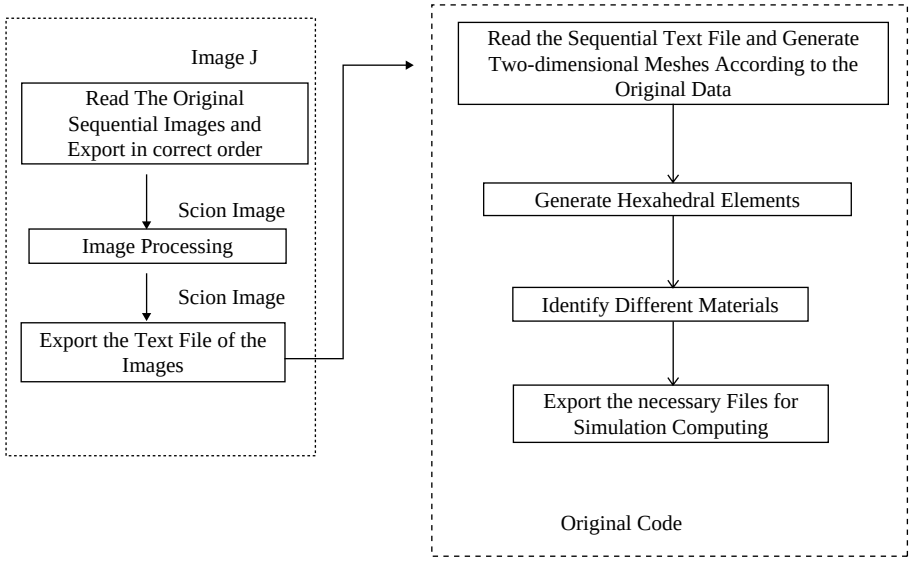

Figure 5.
The Flowchart for mesh generation from medical images

3.4 Identification of blood vessels

Recognizing the position of a large blood vessel in the MR images of the finger is slightly difficult due to the small size of the vessels. Hence, we first chose MR images for the base of the finger, where the diameter of the vessel is larger and easier to judge. Next, the position of the center of the arteries was detected and the information was added to the corresponding four-node FE model. Furthermore, the relative position of the arteries with respect to the edge of the bone in the FE model was recorded, and the same relative position of the arteries was used in the other four-node FE models. Thus, the 3D FE network of the arteries was generated. It was assumed that the veins were in the neighborhood of the arteries and that they had the same diameter as that of the arteries. We also assumed that blood vessels with a diameter smaller than that of the large artery were the fluid phase in the porous media.

4. Computation results

The thermophysical properties are listed in Table II; these properties were obtained from references (Shitzer *et al.*, 1997; Shih *et al.*, 2003). It was considered that tissue

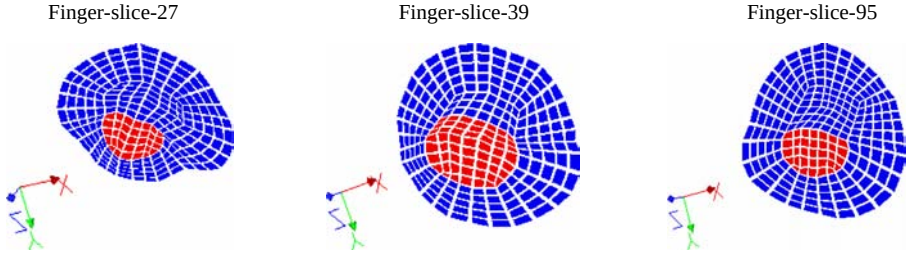

Figure 6.
Two-dimensional FE meshes generated from MR cross-sectional images

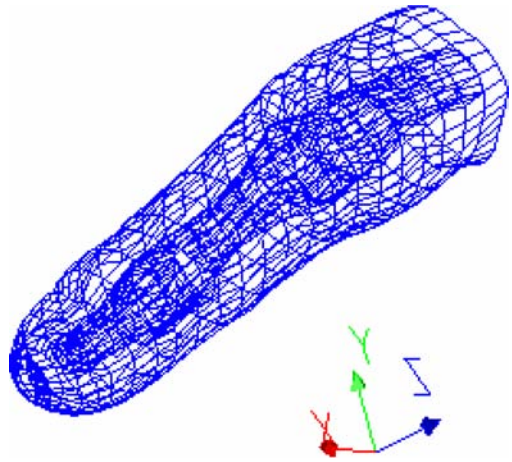

Figure 7.
3D FE network of the human finger

porosity does not normally exceed 0.6 (Nield and Bejan, 1998). Based on the data in Nield and Bejan (1998), we defined the porosity in the bone, tendon, skin, and fingertip as 0, 0.1, 0.2, and 0.3, respectively. Owing to the large density of the vessels at the fingertip, the porosity was assigned a larger value. Tissue permeability was defined as $10^{-13}\,m^2$ (Nield and Bejan, 1998).

The computational code was validated with several simple shapes. Figure 8(a) shows a long narrow bar and Figure 8(b) shows the temperature distribution in the bar when a given temperature boundary condition and a given heat transfer coefficient were assigned on two opposite sides. Another validation was carried out in the shape as Figure 9(a), where two small tubes were embedded in a solid. This shape can be considered as one part of living tissue with two countercurrent vessels. The computed capillary pressure distribution in the tissue is shown in Figure 9(b).

Figure 10 shows the variation of pressure in the large arteries and veins in the finger, and it was computed by the one-dimensional blood flow model. It can be observed that the pressure difference is greater in the artery, whereas there is only a slight difference in the vein. These data were given to nodes that represent the arteries and veins in the FE model and the pressure was set such that it varied along the blood flow direction but did not change in the direction normal to the flow direction. The inflow velocities in the finger artery and vein are 19 and 3.5 cm/s, respectively, according to the computation results obtained from the one-dimensional model, and the Reynolds number in the computation is 50 when the arterial velocity is the reference

	Bone	Tendon	Skin	Blood
ρ (kg/m^3)	1,418	1,270	1,200	1,100
c (J/kgK)	2,094	3,768	3,391	3,300
λ (W/mK)	2.21	0.35	0.37	0.50

Table II.
Physical properties and blood perfusion rates of tissues

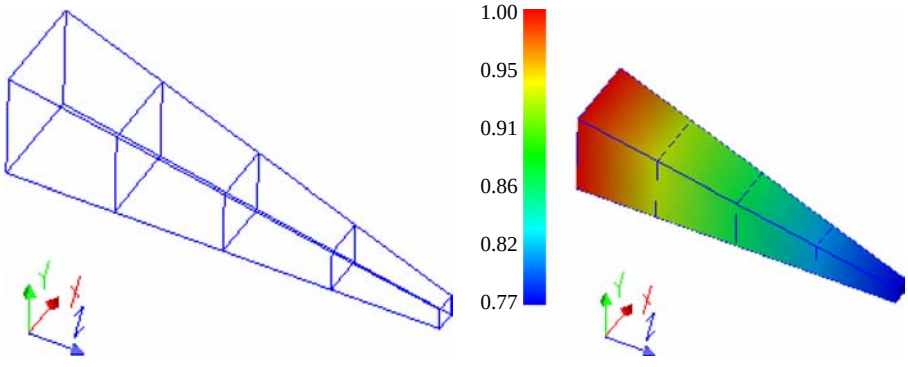

Figure 8.
(a) The long narrow bar for the validation; (b) temperature distribution in the bar

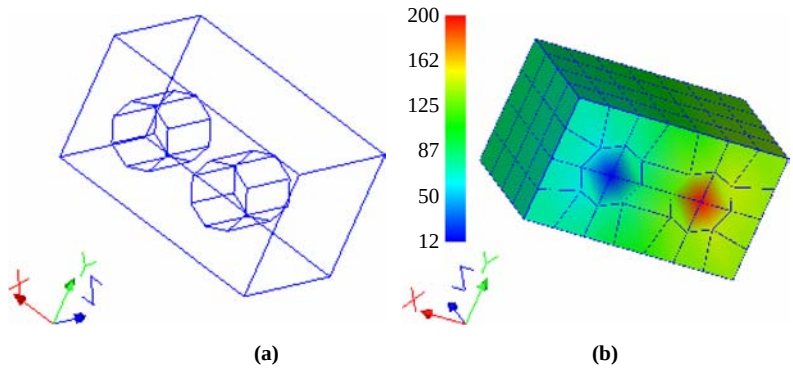

Figure 9.
(a) A test cube with two small vessels; (b) the images after the image segmentation

velocity. Since the computed velocity along the flow direction slightly changes in large vessels, it is assigned to the blood nodes with uniform values.

Figure 11(a)-(b) shows the computed capillary pressure of the finger in different cross-sectional areas. It can be seen that the capillary pressure is between the values of pressure in large artery and vein. Figure 12(a)-(b) shows the flow distribution of the finger in different position. It can be seen that blood flows in the tissue between the large arteries and veins; however, there is almost no blood flow in the tissue between the two large arteries. Furthermore, the blood flow in the fingertip is greater than that in the basal part. In addition, in some areas, the blood flow is in the direction normal to the skin surface, and in other areas, the blood flow is parallel to the skin surface. Therefore, we can identify the thermally significant and insignificant vessels easily.

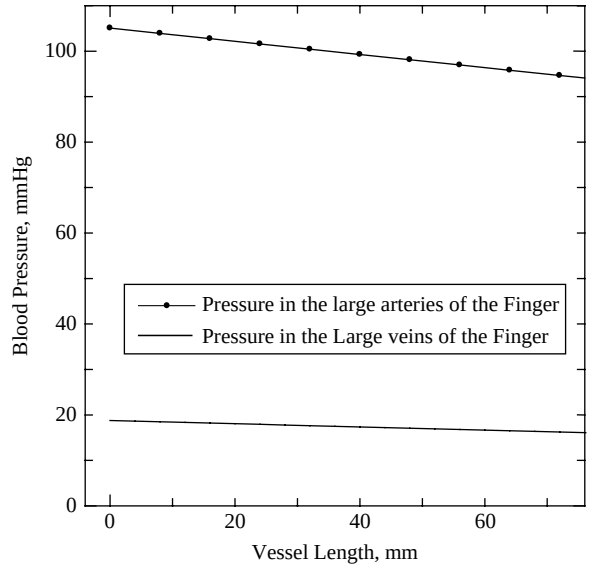

Figure 10.
Pressure distribution in axial direction of blood flow in large arteries and veins of finger

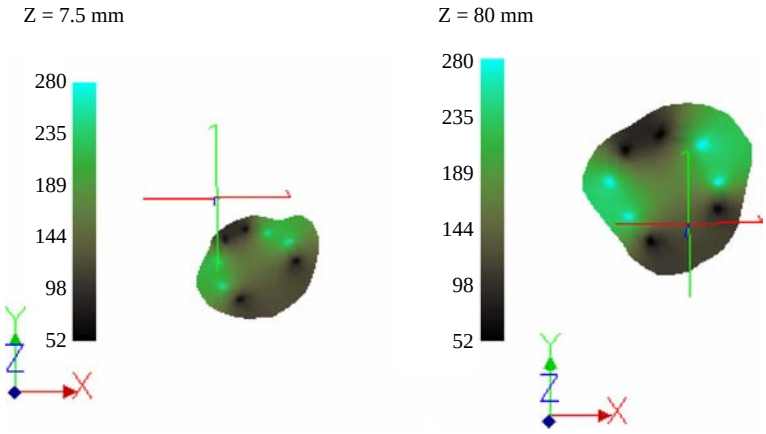

Figure 11.
Capillary pressure distribution in different positions

The flow distribution also shows agreement with the anatomical structure of microvessels.

Figure 13 shows the temperature distribution in the cross-sectional areas of the finger when it was exposed to air. Convective heat transfer can be observed between large arteries and veins. In the areas near the large vessels where there are more thermally significant capillaries, the tissue temperature is distinctly higher. In the fingertip, the tissue and skin surface temperature are higher due to more blood flow.

Figure 14 shows the skin temperature distribution when the blood is perfused and not perfused in the tissue. It can be seen that the blood affects the skin temperature in the fingertip more obviously, which means that blood plays a more important role thermally at the fingertip.

Figure 15(a) shows the skin temperature profile from the fingertip to the basal part of the finger in two different places. It can be seen that the temperature at the fingertip is generally higher than that in the basal part of the finger, and there are fluctuations in the two profiles. Figure 15(b) and (c) shows the measured skin temperature profiles

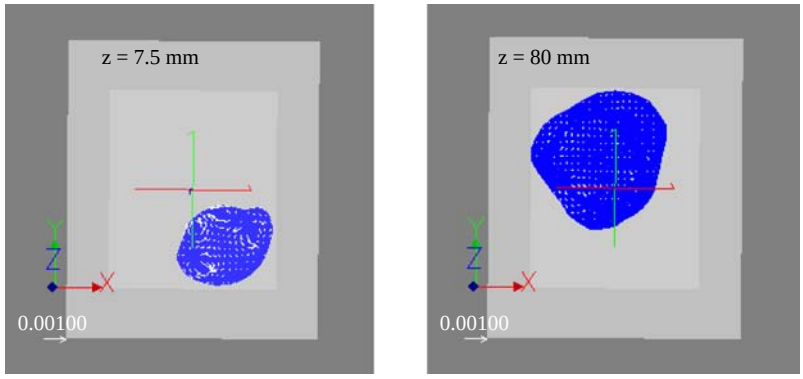

Figure 12.
Blood flow distribution in tissue in different cross-sectional areas

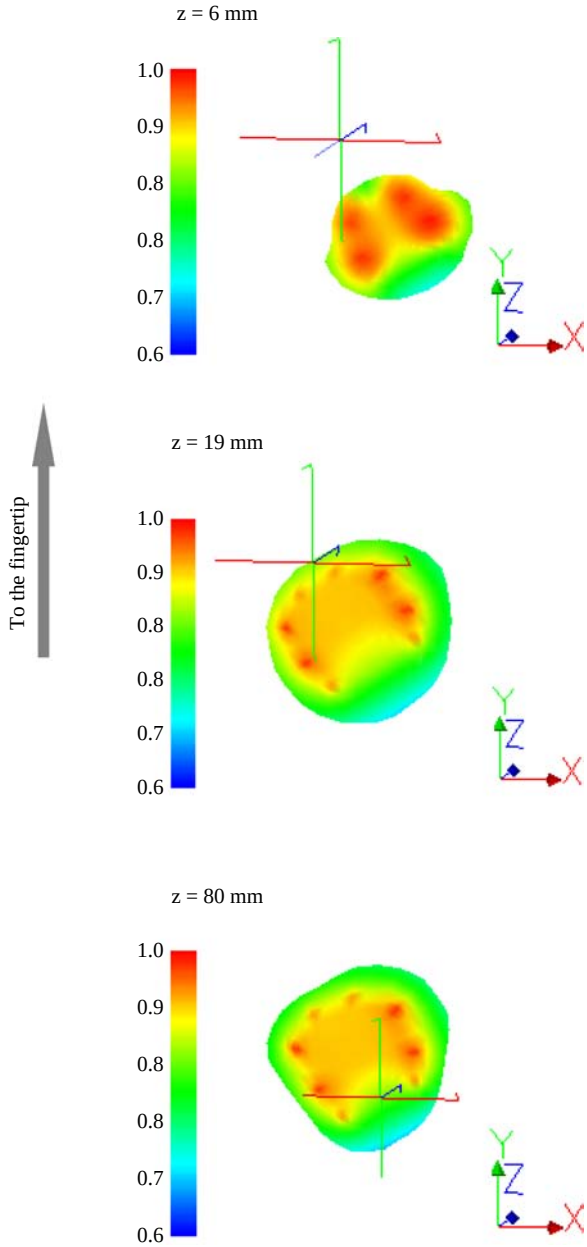

Figure 13.
Temperature distribution in different cross-sectional areas of finger while it is exposed to air

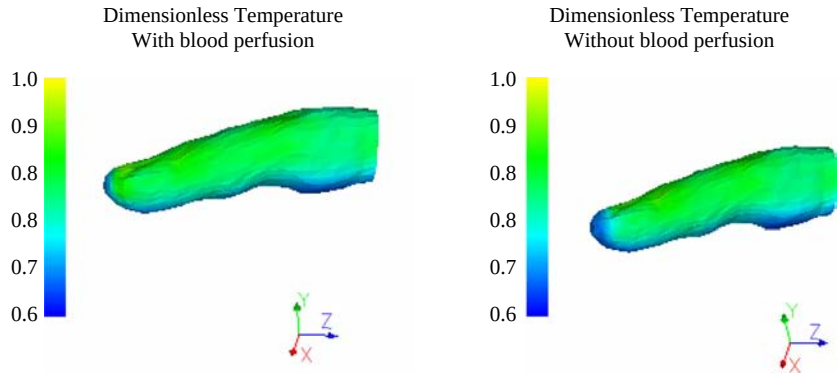

Figure 14.
Skin temperature distribution for different blood perfusions

from the fingertip to the basal part for different subjects. It can be seen that the variation tendency of the simulated results is in agreement with that of the measurements.

5. Discussion and conclusions

In this study, we divided the blood flow in the tissues into two groups: one is blood flow in large vessels (the diameter of the vessels is generally larger than or equal to 1 mm) and the other is blood flow in microvessels. We used a one-dimensional thermofluid model in an elastic tube to describe the blood flow in large vessels and the Darcy model to model the flow in porous media to describe the blood flow in microvessels. The energy equation in porous media was used to model the heat transfer in the tissue. The computed results have shown that the simulated blood flow through tissues is qualitatively in agreement with the anatomical structure and the measurement. Since information on the local blood flow has been obtained from the one-dimensional flow and Darcy models, the thermal effect of different vessels can be evaluated through the energy equation without other parameters.

Another characteristic of this study is that the image-based modeling method was employed to construct the FE model. Since the realistic geometry can be constructed from the medical images directly, we can simulate the blood flow and heat transfer in a more realistic condition. This simulation system can be extended to apply it to analyzing other heat transfer problems in other living tissue.

One limitation of the computational system is that it cannot simulate heat transfer phenomena in the transient state because we assumed that the blood temperature in the tissue achieved equilibrium with the tissue temperature. There is a need to consider the blood temperature and tissue temperature by separate equations so that transient bioheat transfer phenomena can be simulated.

In summary, the simulated system including the one-dimensional hemodynamic modeling, the heat transfer modeling basing on the porous media theory, and image-based geometric modeling provides favorable results in analyzing blood flow and heat transfer problems in living tissues. It is believed that based on a similar concept, the nervous system can also be modeled and more challenging problems with regard to human physiological behavior can be explored.

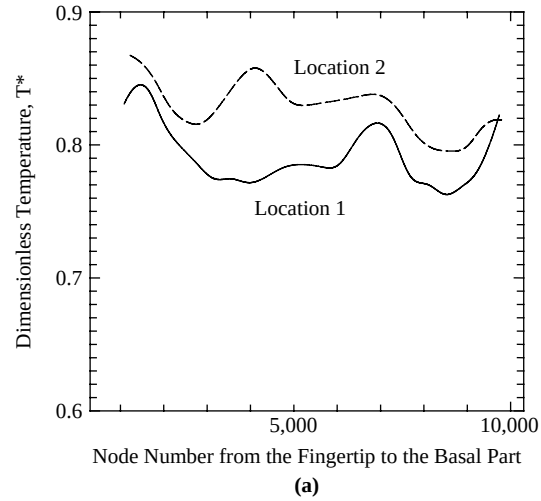

(a)

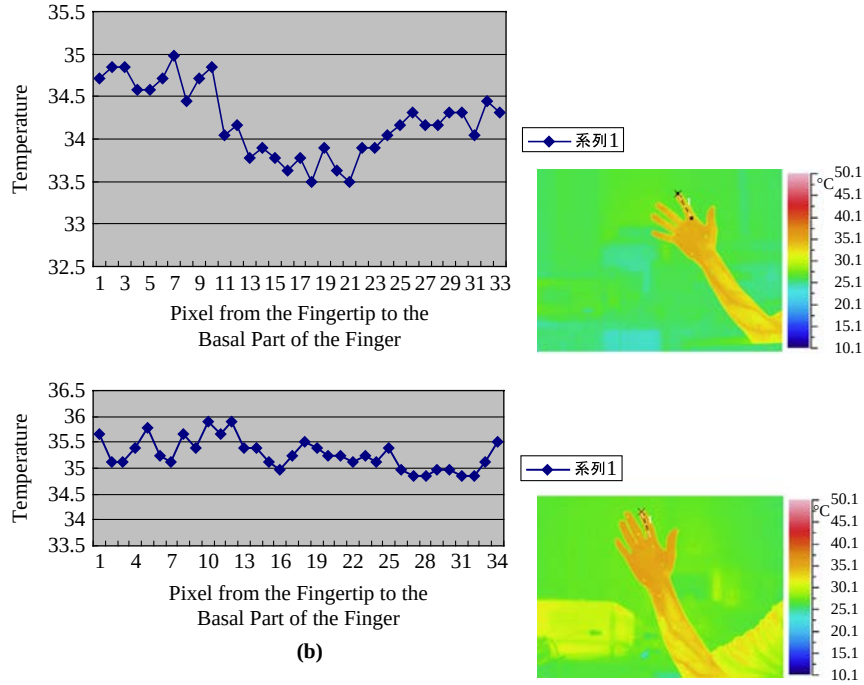

(b)

Figure 15.
(a) Simulated skin temperature profile from the fingertip to the basal part; (b) measured skin temperature profile from the fingertip to the basal part for subject 1 and subject 2

References

ASHRAE (1997), *ASHRAE Fundamentals Handbook*, ASHRAE Press, Atlanta, GA.

Bornmyr, S. and Svensson, H. (1991), "Thermography and laser-Doppler flowmetry for monitoring changes in finger skin blood flow upon cigarette smoking", *Clinical Physiology*, Vol. 11, pp. 135-41.

Chen, M.M. and Homles, K.R. (1980), "Microvascular contributions in tissue heat transfer", *Annals of the New York Academy of Sciences*, Vol. 335, pp. 137-50.

Cho, O.K., Kim, Y.O., Mitsumaki, H. and Kuwa, K. (2004), "Noninvasive measurement of glucose by metabolic heat conformation method", *Clinical Chemistry*, Vol. 50 No. 10, pp. 1894-8.

Clark, R.P. and Edholm, O.G. (1985), *Man and His Thermal Environment*, Edward Arnold (Publishers) Ltd, London.

Fukuda, S., Sakai, N. and Shimawaki, S. (2005), "Numerical simulation of mechanical deformation of three-dimensional human fingertip model constructed from CT data", *Proceedings of the 16th JSME Conference on Frontiers in Bioengineering*, *Kusatsu, November 10-11*.

He, Y., Liu, H. and Himeno, R. (2004), "A one-dimensional thermo-fluid model of blood circulation in upper limb of man", *International Journal of Heat and Mass Transfer*, Vol. 47 Nos 12/13, pp. 2735-45.

He, Y., Liu, H., Himeno, R., Sunaga, J., Kakusho, N. and Yokota, H. (2006), "Finite element analysis of blood flow and heat transport in the human finger", International Heat Transfer Conference IHTC-13, Sydney, August.

Khaled, A.R.A. and Vafai, K. (2003), "The role of porous media in modeling flow and heat transfer in biological tissues", *Int. J. Heat Mass Transfer*, Vol. 46, pp. 4989-5003.

Koscheyev, V.S., Leon, G.R., Paul, S., Tanchida, D. and Linder, I.V. (2000), "Augmentation of blood circulation to the fingers by warming distant body areas", *European Journal of Applied Physiology*, Vol. 82, pp. 103-11.

Li, C.W. and Cheng, H.D. (1993), "A nonlinear fluid model for pulmonary blood circulation", *J. Biomechanics*, Vol. 26 No. 6, pp. 653-64.

Ling, J.X., Young, I.R. and DeMeester, G. (1995), "A finite element model for determining the cooling effects of water bags on the temperature distributions of a human leg", *Advances in Heat and Mass Transfer in Biotechnology, ASME*, HTD-Vol. 322/BED-Vol. 32, pp. 69-71.

Nield, D.A. and Bejan, A. (1998), *Convection in Porous Media*, 2nd ed., Springer Publishing Company, New York, NY.

Nketia, P. and Reisman, S. (1997), "The relationship between thermoregulatory and hemodynamic responses of the skin to relaxation and stress", *Proceedings of the IEEE, 23rd Northwest Bioengineering Conference, IEEE, New York, NY*, pp. 27-8.

Olufsen, M.S., Peskin, C.S., Kim, W.Y., Pedersen, E.R., Nadim, A. and Larsen, J. (2000), "Numerical simulation and experimental validation of blood flow in arteries with structured-tree outflow conditions", *Annals of Biomedical Engineering*, Vol. 28, pp. 1281-99.

Pennes, H.H. (1948), "Analysis of tissue and arterial blood temperatures in the resting human forearm", *Journal of Applied Physiology*, Vol. 1 No. 2, pp. 93-122.

Reynolds, H.M., Smith, N.P. and Hunter, P.J. (2006), "Construction of an anatomically accurate geometric model of the forearm and hand musculo-skeletal system", *Proceedings of the 26th Annual International Conference of the IEEE EMBS, San Francisco, CA, September*, pp. 1829-32.

Salloum, M., Ghaddar, N. and Ghali, K. (2005), "A new, transient bio-heat model of the human body", *Proceedings of HT2005, 2005 ASME Summer Heat Transfer Conference*.

Sheng, C., Sarwal, S.N., Watts, K.C. and Marble, A.E. (1995), "Computational simulation of blood flow in human systemic circulation incorporating an external force field", *Medical & Biological Engineering & Computing*, Vol. 33, pp. 8-17.

Shih, T.C., Kou, H.S. and Lin, W.L. (2003), "The impact of thermally significant blood vessels in perfused tumor tissue on thermal dose distributions during thermal therapies", *Int. Comm. Heat Mass Transfer*, Vol. 30 No. 7, pp. 975-85.

Shitzer, A., Stroschein, L.A., Vital, P., Gonzalez, R.R. and Pandolf, K.B. (1997), "Numerical analysis of an extremity in a cold environment including countercurrent arterio-venous heat exchange", *Trans. ASME, Journal of Biomechanical Engineering*, Vol. 119, pp. 179-86.

Takemori, T., Nakajima, T. and Shoji, Y. (1995), "A fundamental model of the human thermal system for prediction of thermal comfort", *Trans. JSME*, Vol. 61 No. 584, pp. 1513-20.

Weibaum, S. and Jiji, L.M. (1985), "A new simplified bioheat equation for the effect of blood flow on local average tissue temperature", *J. Biomech. Eng.*, Vol. 107, pp. 131-9.

Wulff, W. (1974), "The energy conservation equation for living tissue", *IEEE Transactions on Biomedical Engineering*, pp. 494-5.

Xuan, Y.M. and Roetzel, W. (1997), "Bioequation of the human thermal system", *Chem. Eng. Technol.*, Vol. 20, pp. 269-76.

Yokoyama, S. and Ogino, H. (1985), "Developing computer model for analysis of human cold tolerance", *The Annals of Physiological Anthropology*, Vol. 4 No. 2, pp. 183-7.

Zagzoule, M. and Marc-Vergnes, J. (1986), "A global mathematical model of the cerebral circulation in man", *J. Biomechanics*, Vol. 19 No. 12, pp. 1015-22.

(The Appendix Figure follows overleaf.)

Appendix. The original main program for generating brick element

```
      ********************************************************************
c     |     The program is written for transferring the mri color data to be
c     |     three dimensional FEM node and element data
c     |     by Ying HE
c     |   June. 2006   revised version
c     ********************************************************************
c     ------Read the color text data from edit MRI dcm file-------------------
c     ------The dcm file is firstly exported to be the txt file with brightness information------
c     ------by image processing software Scion image ----
c     ------The common characteristic: 11 groups of data----------------
c     ------to express the geometry of fingercross section---------------
#include"control.h"
      implicit none
c--------color: the color brightness of every pixel
      integer i,j,k,id
       integer iz
c
      integer nskin1,nskin2,nskin3,nskin4
      integer ntendon1,ntendon2
      integer nbone1,nbone2,nbone3,nbone4,nbone5
       real*8   xorig,yorig
       dimension xorig(gpoint,Ngroup),yorig(gpoint,Ngroup)

c
c ----define the file name----------0
      character*14 seriname
      integer tendiv,skindiv
      integer nout,nin,inside
       real*8 xout,yout
       dimension xout(gpoint),yout(gpoint),inside(gpoint)
c
c-----The parameter related to the node and element information
      integer numnod,numelem2,numelem1,numelemt,prenumnod
       real*8   nx,ny,nz
       dimension nx(NoNode),ny(NoNode),nz(NoNode)
       integer nop1,nop2,nophex
c-----material: element material
      integer material1,material2,materialt
       dimension nop1(4,sElem),nop2(4,sElem),nophex(8,NoElem)
       dimension material1(sElem),material2(sElem),materialt(NoElem)
       real*8     nmarker
       dimension nmarker(NoElem)
c-----boundary marker: bemarker
      integer bemarker,sbemarker1,sbemarker2
       dimension bemarker(NoElem),sbemarker1(NoElem),sbemarker2(NoElem)
c-----the node number in every line----------------------------
      integer   line,linet1,linet2,lines
       dimension line(Nline,gpoint),lines(gpoint,gpoint)
       dimension linet1(Nline,gpoint),linet2(Nline,gpoint)
c
c-------------------------------------------------------------------------------
       numnod=0.0
       numelemt=0
      do i=1,24
c---count element at every cross section-----
       if(i.le.2) then
         iz=slicenum+(i-1)*1
       else if (i.ge.3.and.i.le.5) then
         iz=slicenum+(i-2)*2
       else
         iz=slicenum+(i-4)*4
       end if

       call mkname(iz,seriname)
```

(*continued*)

Figure A1.

```
c-----Read the pixcel data---------------------------------------
      call idpixel(nskin1,nskin2,nskin3,nskin4,ntendon1,ntendon2,
     +           nbone1,nbone2,nbone3,nbone4,nbone5,xorig,yorig,seriname)

c-----It is not necessary for the 1st two slices
c       if(i.gt.1) then
c----let the characteristic points be in the correct order----------
      call   correctorder(nskin1,xorig,yorig)
c----the total points to show the outside geometry
      call   outgeometry(nskin1,nskin2,nskin3,nskin4,xorig,yorig,
     +         xout,yout,nout)
c       end if
c
c------the characteristic points for showing the geometry----------
      open(1,File='testdata.dat')
       do id=1,12
        do,j=1,14
          write(1,35) j,xorig(j,id),yorig(j,id)
35        format(i10,2f15.5)
        end do

       end do
       do id=1,nout
          write(1,40) id, xout(id),yout(id)
40      format(i10,2f15.5)
       end do
       close(1)
c-----Node generation-------------------------------------------

c-----tendiv and skindiv will be written in an input file
       tendiv=4
       skindiv=11

c
       call bonenode(nbone1,nbone2,nbone3,
     +                    xorig,yorig,nx,ny,numnod,line)

c       if(i.gt.1) then
       call tendonnode(tendiv,ntendon1,ntendon2,
     +           xorig,yorig,nx,ny,numnod,line,linet1,linet2)

c
       call insidegeometry(nbone1,nbone2,nbone3,tendiv,
     +                line,linet1,linet2,inside,nin)

       call skinnode(skindiv,inside,nin,xout,yout,nout,
     +         nx,ny,numnod,lines)
c       end if
c
c-----determine the coordinate of every node in z direction
       if(i.eq.1) then
       call zdirectionfirst(line,linet1,linet2,
     +           lines,nout,numnod,tendiv,skindiv,ntendon2,
     +           iz,nx,ny,nz,prenumnod)

       else
       call zdirection(iz,prenumnod,numnod,nz)
       end if
c-----regulate z in the bone joint position,
c-----Currently, don't use this part,Aug.3 2006
c       call zbonejoint(linet1,linet2,tendiv,ntendon1,iz,nz)

c-----make element in one cross area----------------------------

       call mkelem(iz,nbone1,nbone2,ntendon1,tendiv,skindiv,
     +                nout,line,linet1,linet2,lines,numelem2,nop2,
     +                material2)
```

Figure A1. (*continued*)

```
c----identifiy the blood part--Sep. 6 2006----------
c----determine nmarker for boundary condition----------
          if(i.gt.5) then
          call bloodvessel(skindiv,lines,nx,ny,nout,numnod,
         +                 prenumnod,nop2,numelem2,nmarker,material2)
          end if
c----determine nmarker and bemarker
c----Here, numnod --> prenumnod to go to the next slice
c----After finishing making marker, the work will be shifted in another slice
          call mkmarker(iz,nout,lines,prenumnod,numnod,numelem2,
         +              nop2,nmarker,sbemarker2)
c-----make 3D element, brick element-----
          if(i.eq.1) then
            numelem1=numelem2
            call putind(numelem1,nop1,nop2)
            call putind(numelem1,material1,material2)
            call putind(numelem1,sbemarker1,sbemarker2)

           else

            call mkelembrick(numelem1,nop1,material1,numelem2,nop2,material2,
         +       numelemt,nophex,materialt,sbemarker1,bemarker)
            numelem1=numelem2
            call putind(numelem1,nop1,nop2)
            call putind(numelem1,material1,material2)
            call putind(numelem1,sbemarker1,sbemarker2)

           end if

          end do
c.........output element,node,boundary, and initial data
          call computoutput(nx,ny,nz,numnod,numelemt,nophex,
         +       nmarker,materialt,bemarker)
c---data for avs visualization
          call output(nx,ny,nz,numnod,numelemt,nophex,materialt,nmarker)

          write(*,*) 'finished'
          stop
          end
```

Figure A1.

Corresponding author
Ying He can be contacted at: yhe@ustc.edu.cn